Check for updates

AGU ADVANCING EARTH AND SPACE SCIENCES

Geophysical Research Letters

RESEARCH LETTER
10.1029/2023GL106829

Decoding the Interplay Between Tidal Notch Geometry and Sea-Level Variability During the Last Interglacial (Marine Isotope Stage 5e) High Stand

N. Georgiou[1,2], P. Stocchi[3,4], E. Casella[1], and A. Rovere[1,5]

[1]Ca' Foscari University of Venice, Department of Environmental Sciences, Informatics and Statistics, Mestre (VE), Italy, [2]University of Patras, Department of Geology, Patra, Greece, [3]Dipartimento di Scienze Pure e Applicate (DiSPeA), Università degli Studi di Urbino "Carlo Bo", Urbino, Italy, [4]I4CCS Institute for Climate Change Solutions, Frontone (PU), Italy, [5]MARUM, Center for Marine Environmental Sciences, University of Bremen, Bremen, Germany

Key Points:

- Cliff erosion modeling and Monte Carlo analysis indicate tidal notch geometry can offer a continuous record of past sea level variability
- The geometry of Orosei's tidal notch, Italy can be replicated through simultaneous or asynchronous Antarctic–Greenland ice melting scenarios
- The morphology of the Last Interglacial notch is more efficiently replicated using higher-than-present erosion rates and a 6 m sea-level peak

Supporting Information:

Supporting Information may be found in the online version of this article.

Correspondence to:

N. Georgiou,
nikos.georgiou@unive.it

Citation:

Georgiou, N., Stocchi, P., Casella, E., & Rovere, A. (2024). Decoding the interplay between tidal notch geometry and sea-level variability during the Last Interglacial (Marine Isotope Stage 5e) high stand. *Geophysical Research Letters*, *51*, e2023GL106829. https://doi.org/10.1029/2023GL106829

Received 18 OCT 2023
Accepted 5 MAR 2024

Author Contributions:

Conceptualization: N. Georgiou, P. Stocchi, A. Rovere
Data curation: N. Georgiou
Formal analysis: N. Georgiou
Funding acquisition: A. Rovere
Investigation: N. Georgiou, P. Stocchi, E. Casella, A. Rovere
Methodology: N. Georgiou, P. Stocchi, E. Casella, A. Rovere
Project administration: A. Rovere
Resources: A. Rovere
Software: N. Georgiou, P. Stocchi
Supervision: A. Rovere

© 2024. The Authors.
This is an open access article under the terms of the Creative Commons Attribution-NonCommercial-NoDerivs License, which permits use and distribution in any medium, provided the original work is properly cited, the use is non-commercial and no modifications or adaptations are made.

Abstract Relic coastal landforms (fossil corals, cemented intertidal deposits, or erosive features carved onto rock coasts) serve as sea-level index points (SLIPs), that are widely used to reconstruct past sea-level changes. Traditional SLIP-based sea-level reconstructions face challenges in capturing continuous sea-level variability and dating erosional SLIPs, such as tidal notches. Here, we propose a novel approach to such challenges. We use a numerical model of cliff erosion embedded within a Monte Carlo simulation to investigate the most likely sea-level scenarios responsible for shaping one of the best-preserved tidal notches of Last Interglacial age in Sardinia, Italy. Results align with Glacial Isostatic Adjustment model predictions, indicating that synchronized or out-of-sync ice-volume shifts in Antarctic and Greenland ice sheets can reproduce the notch morphology, with sea level confidently peaking at 6 m and only under a higher than present erosion regime. This new approach yields insight into sea-level trends during the Last Interglacial.

Plain Language Summary Scientists typically investigate the position of sea level in geological time using the elevation, age, and characteristics of fossil marine organisms living in shallow water (e.g., coral reefs), beach deposits, or erosional features that were formed near the sea level. However, these indicators offer only fragmented, if not only point-like information in time and not a continuous sea-level record. To overcome this issue, we use a numerical model that reconstructs the shape of tidal notches (i.e., indentations created close to sea level in carbonate cliffs). We compare model-generated notch shapes with the real shape of the tidal notch, and we produce a set of continuous sea-level histories that are more likely to have produced one of the best-preserved fossil tidal notches in the Orosei Gulf, Sardinia, Italy, carved during the Last Interglacial highstand, 125.000 years ago. Our findings suggest that whether the ice sheets in Antarctica and Greenland melted at the same time or separately, both scenarios could reproduce the actual shape of the tidal notch we observe at present. Our findings indicate that the erosion rate during that period was higher than present and the sea level is very likely to have reached up to 6 m.

1. Introduction

Coastal features such as fossil corals (Chutcharavan and Dutton, 2021) or cemented intertidal beach deposits (Goodwin et al., 2023) formed at or close to sea level during past Interglacials can be used as sea-level index points (SLIPs), providing essential insights on past sea-level histories and hence on the dynamics related to the waxing and waning of ice sheets during periods that serve as analogs for the near future (Dutton et al., 2015). The conventional method of gathering paleo sea-level data from SLIPs involves determining their elevation and relationship with the former sea level (Shennan, 2015), dating them via radiometric methods (such as U-series), and ultimately reconstructing a relative sea level (RSL) curve from multiple SLIPs, detailing the local interplay by changing sea level and land motions of non-climatic origin (Kopp et al., 2009). Despite its widespread application across thousands of global sites (Rovere et al., 2023), this approach has two major drawbacks.

First, SLIPs at one location are hardly continuous through time, and are often remnants of the past highstand peaks, providing little insight into the variability of sea level throughout the Interglacial (with the exception of specific occurrences involving speleothems and fossil coral reefs). Second, SLIPs such as shore platforms (Trenhaile, 2001) or tidal notches (Antonioli et al., 2018) are ubiquitous but erosional in nature, with their dating usually relying on indirect methods, specifically through stratigraphic correlation with deposits of established

19448007, 2024, 6, Downloaded from https://agupubs.onlinelibrary.wiley.com/doi/10.1029/2023GL106829 by CochraneItalia, Wiley Online Library on [19/03/2024]. See the Terms and Conditions (https://onlinelibrary.wiley.com/terms-and-conditions) on Wiley Online Library for rules of use; OA articles are governed by the applicable Creative Commons License

Validation: N. Georgiou
Visualization: N. Georgiou, E. Casella
Writing – original draft: N. Georgiou
Writing – review & editing: P. Stocchi, E. Casella, A. Rovere

age. In this study, we suggest a novel solution that may help overcome the continuity and dating limitations of the traditional paleo sea-level analysis by reversing the conventional approach.

We begin by surveying with high-precision methods the morphology of a very well-preserved, laterally continuous tidal notch that formed during the warmest peak of Marine Isotope Stage 5 (MIS5e), the Last Interglacial (LIG–125 ka BP) in the Orosei Gulf (Sardinia, Italy, NW Mediterranean). The Sardinian coast contains a multitude of MIS 5e sea-level indicators as summarized in Cerrone et al. (2021). MIS 5e marine deposits containing Glycimeris shells were detected at an elevation of +1.8 m on Tavolara island (Belluomini et al., 1986), and serve as the sole direct sea-level indicator on the eastern coast of Sardinia, while the presence of MIS 4-2 aeolianites covering the notch (Antonioli & Ferranti, 1992) further supports that the Orosei notch was formed during the LIG. On the SE Sardinian coast, MIS 5e beach deposits were found at an elevation of 6.3 ± 0.47 m (Hearty, 1986). A tidal notch is an indentation carved on steep carbonate cliffs: an active tidal notch is typically located near the mean sea level. In regions with micro- and meso-tidal ranges, like the Mediterranean Sea, tidal notches exhibit their greatest concavity proximal to the intertidal zone (Antonioli et al., 2018). Their genesis is attributed to a combination of active processes such as bioerosion, wetting and drying cycles, mechanical wave erosion, and hyperkarst (Trenhaile, 2015), which determine the rate of erosion. The width of the tidal notches, defined as the distance between their floor and roof, is predominantly controlled by the tidal range (Pirazzoli et al., 1991). Meanwhile, sea level stabilization or slow-down time, and whether the site is exposed or not (Vacchi et al., 2022) determines the incision depth and the width of the tidal notches, shaping the overall notch morphology (Trenhaile, 2016). Hence, fossil notches are frequently employed as SLIPs (Antonioli et al., 2015; Pirazzoli, 1986, 2005).

By incorporating a numerical model of cliff erosion (modified after Schneiderwind et al., 2017) with sea level as a fluctuating parameter, we use a Monte-Carlo approach (Eckhardt, 1987) to fit the model results with the measured notch geometry while accounting for the active processes involved in notch formation (Georgiou et al., 2020). We show that our best-fitting results closely align with the relative sea level predicted by Glacial Isostatic Adjustment (GIA) models at this locality (Stocchi et al., 2018). By imposing higher-than-present cliff erosion rates, we can force the model to reproduce two, three, or more separate sea level peaks, which can be attributed to ice-volume change asynchrony between the Antarctic and Greenland ice sheets (Dumitru et al., 2023; Rohling et al., 2008, 2019). Using this modeling approach, we provide a novel perspective into the use of erosional SLIPs, which might be of use to unravel intra-highstand sea-level variability.

2. Methodological Approach

2.1. Photogrammetric Data Collection and Evaluation

In summer 2019, the Orosei tidal notch was surveyed with a boat along the cliff, during calm sea and low tide. Cliff photos were taken using a CANON D300 camera, then analyzed with Structure from Motion and Multi-View Stereo (SfM-MVS) techniques via Agisoft Metashape (www.agisoft.com, see Text S1 in Supporting Information S1, Carrivick and Quincey, 2016; Casella et al., 2016; Ullman, 1979). The model was scaled and benchmarked to mean sea level, using the modern notch's inner part as a reference.

The 3D model, imported into ArcGIS 10.1, allowed extraction of notch geometries as cross-profiles (Figures 1a and 2). Notch morphology varies due to local factors affecting depth, initial cliff plane, and notch floor extension. Morphometric analysis of the Digital Elevation Model (DEM) identified poorly preserved segments, influenced by flowstone-like calcite formations, differential erosion, and rockfalls, using terrain attributes (i.e., slope, aspect, surface roughness) (Florinsky, 2017; Horn, 1981; Olaya, 2009; Sappington et al., 2007) and cliff color distribution (Figure S1, Text S2 in Supporting Information S1). "Measured Notch Profiles" were obtained by averaging the point cloud at 1 m intervals along the *y*-axis.

2.2. Notch Reconstruction Model

Few theoretical models have attempted to simulate the formation of a notch (Evelpidou et al., 2011, 2012; Larson et al., 2010; Pirazzoli, 1986; Trenhaile, 2014, 2015, 2016). To reconstruct the geometry of the measured notch at Orosei we modified the model of Schneiderwind et al. (2017), a numerical model that integrates variables such as sea level change, erosion rate, tidal range, tectonics, and initial cliff inclination. This model employs a quadric polynomial equation (Equation 1) which simulates the development of a tidal notch through a parabola whose

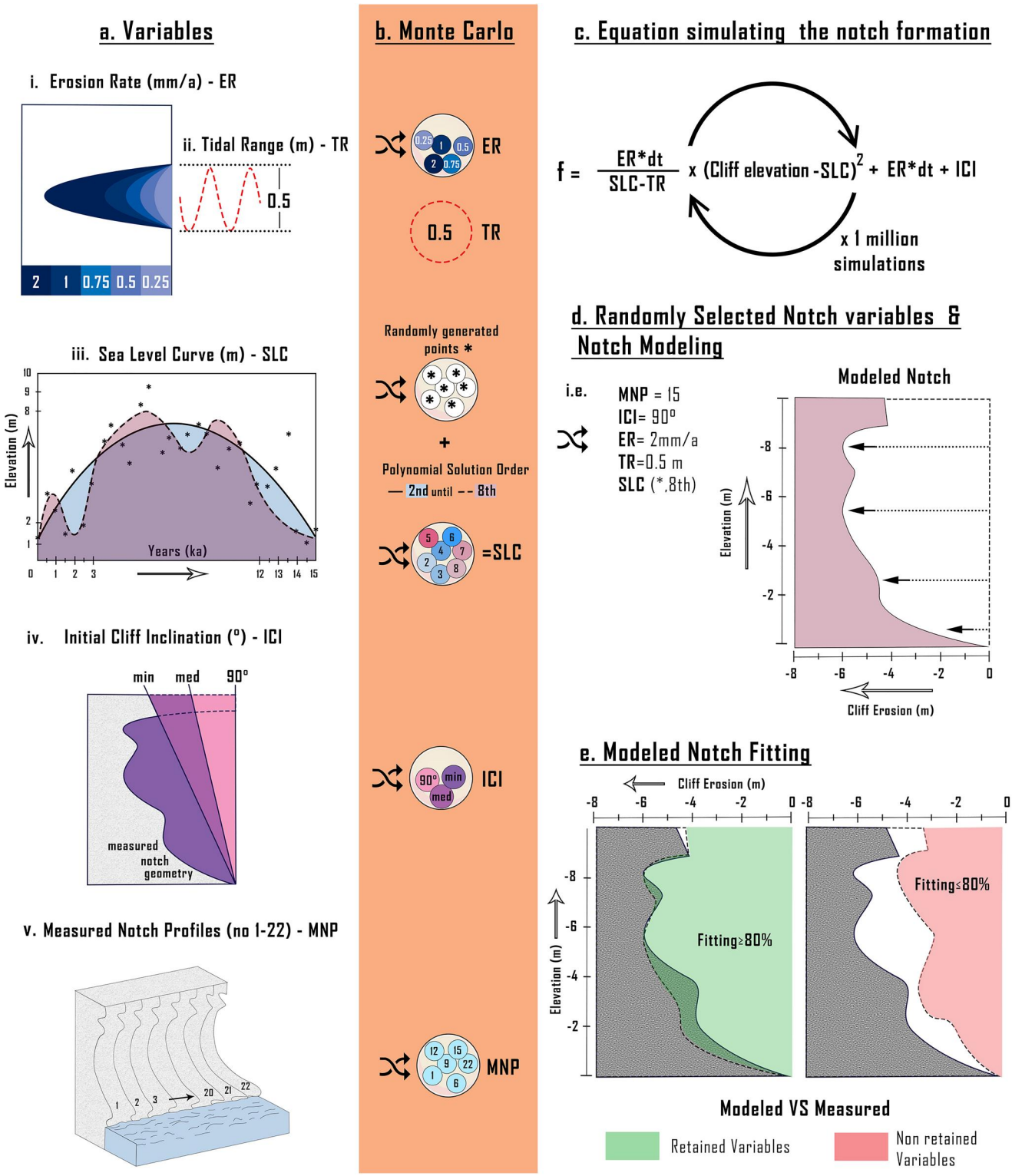

Figure 1. Model Workflow: (a) Variables used in the equation: (i) Erosion Rate range in mm/a, (ii). Tidal Range: 0.5 m (constant), (iii). Sea Level Curve produced through random points interpolation using second to eighth polynomial solution order, (iv). Initial Cliff Inclination where the notch started to form, (v). Measured Notch Profiles (MNPs) measured through SfM-MVS, (b) Randomly Selected Variables through Monte Carlo simulation, (c) Equation used for the notch modeling looped 1 million times, (d) Example of the modeled notch simulated from their random combination, (e) The variables producing a notch fitting higher or equal to 80% to the MNPs were retained (Software available in Georgiou (2023a), https://doi.org/10.5281/zenodo.8407427).

19448007, 2024, 6, Downloaded from https://agupubs.onlinelibrary.wiley.com/doi/10.1029/2023GL106829 by CochraneItalia, Wiley Online Library on [19/03/2024]. See the Terms and Conditions (https://onlinelibrary.wiley.com/terms-and-conditions) on Wiley Online Library for rules of use; OA articles are governed by the applicable Creative Commons License

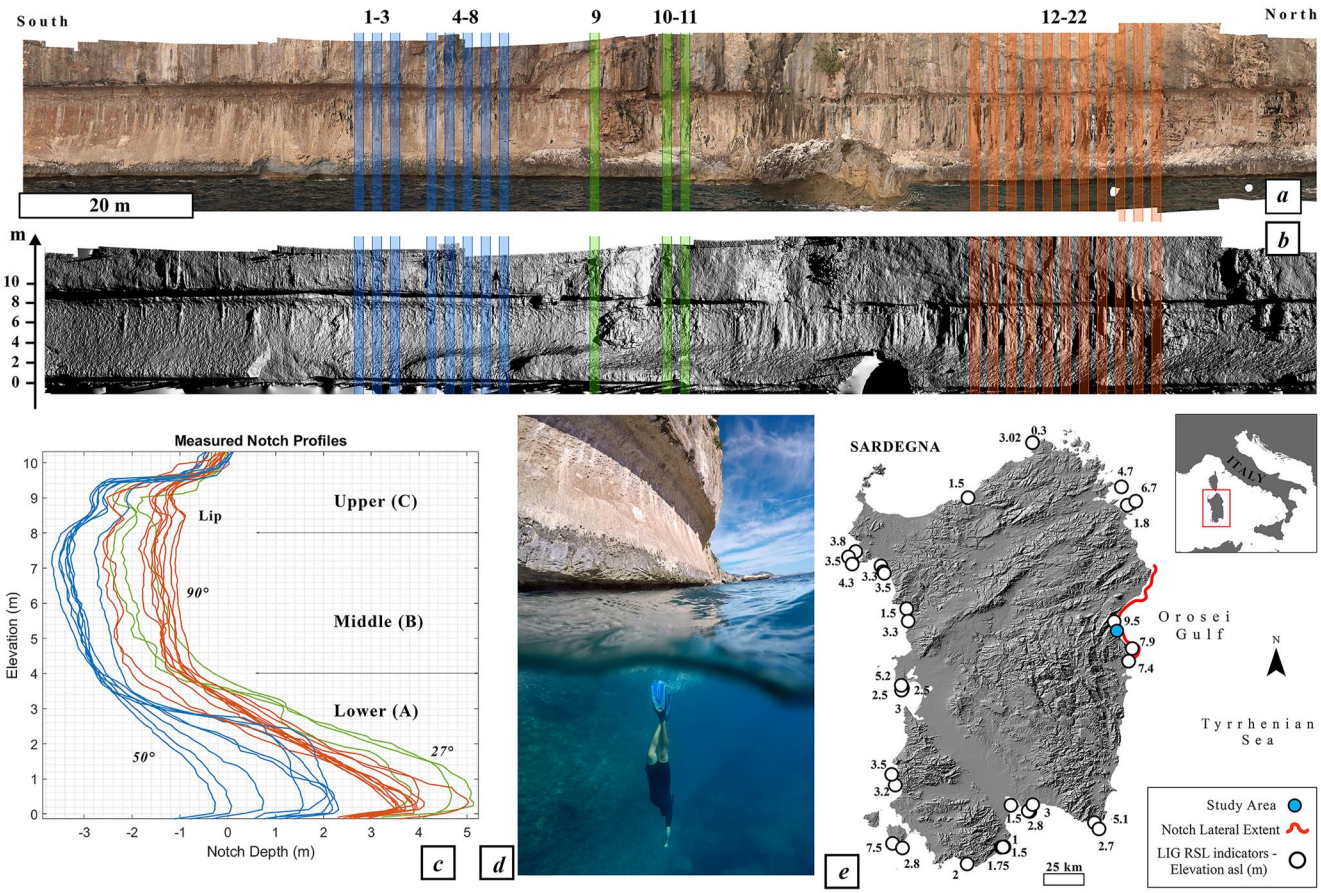

Figure 2. (a) Orthomosaic of the notch on Orosei's limestone cliff, with colored bands indicating MNPs with similar geometry used in the numerical model, (b) 3D hillshade model, (c) MNPs used in the model, (d) "Over-under" photo of notch geometry, (e) Sardinia's hillshade map shows notch extension (red), MIS 5e RSL indicators (white dots) (Rovere et al., 2023), and study area (blue dot).

shape is determined by the variables shown in Figure 1a – (i) Erosion Rate (ER), (ii) Tidal Range (TR), (ii) Sea Level Curves (SLC), (iv) Initial Cliff Inclination (ICI), (v) Measured Notch Profiles (MNP).

$$f = \frac{ER * dt}{SLC - TR} * (cliff\ elevation - SLC)^2 + ER * dt + ICI \quad (1)$$

The parabola's depth, representing the notch depth, is influenced by the ER after 1 yr at mean sea level (Figure 1a-i). The width, defined as the distance between the notch floor and roof, is governed by the TR and the SLC fluctuation (Figure 1a-ii, iii). The initial cliff's inclination, where the parabola forms, varies from vertical to inclined (Figure 1a-iv) depending on the selected notch profile from the field measurements (MNP) (Figure 1a-v). Using this equation in a Monte Carlo loop (Figure 1c), which generates 1 million random combinations of the described variables (example in Figure 1d), and by applying them to Equation 1, 1 million random notch simulations are produced. Notches with a fitting accuracy of at least 80% to the measured ones were retained in each code iteration (Figure 1e). The values selected are described below:

i. Erosion Rate (ER): In our simulation, the depth of the tidal notch is determined by the erosion rate, which is the cumulative effect of all the active erosional processes taking place within the bounds of the tidal cycle. A range of 0.1–2 mm/a of erosion was considered based on micro-erosion measurements and the carving depth of currently forming tidal notches across limestone cliffs in the Mediterranean Sea (Antonioli et al., 2015; Boulton & Stewart, 2015; Evelpidou & Pirazzoli, 2016; Furlani & Cucchi, 2013; Furlani et al., 2014; Pirazzoli & Evelpidou, 2013). ER used in the simulation was selected randomly for each iteration between the

19448007, 2024, 6, Downloaded from https://agupubs.onlinelibrary.wiley.com/doi/10.1029/2023GL106829 by CochraneItalia, Wiley Online Library on [19/03/2024]. See the Terms and Conditions (https://onlinelibrary.wiley.com/terms-and-conditions) on Wiley Online Library for rules of use; OA articles are governed by the applicable Creative Commons License

19448007, 2024, 6, Downloaded from https://agupubs.onlinelibrary.wiley.com/doi/10.1029/2023GL106829 by CochraneItalia, Wiley Online Library on [19/03/2024]. See the Terms and Conditions (https://onlinelibrary.wiley.com/terms-and-conditions) on Wiley Online Library for rules of use; OA articles are governed by the applicable Creative Commons License

following values 0.25, 0.5, 0.75, 1, and 2, and is expressed as the parabolic erosion in millimeters per annum (mm/a).

ii. Tidal Range (TR): The notch width for each annual tidal cycle was determined by the TR which was constant and analogous to the present TR (0.5 m), based on the closest local tide gauge in Cagliari (www.mareografico.it, ISPRA). The analysis assumes consistent TR, as TR variations are more pronounced with regions characterized by shallow shelves (Lorscheid, Felis, et al., 2017), while deeper continental shelves demonstrate reduced susceptibility to tidal range changes under higher MIS 5e sea level conditions.

iii. Sea Level Curves (SLC): The notch's shape was simulated using randomly generated SLCs with predetermined duration and level extents. Random points were generated within a 15 ka time window (mimicking MIS 5e duration, as per Polyak et al., 2018) at intervals of 500 years, ranging from 0 to 10 m elevation, with 10 cm precision (Figure 1a-iii). This range corresponds to the maximum elevation of the Orosei notch above the mean sea level (amsl) and the highest reported during the LIG (Dutton et al., 2015). Each simulation involved interpolating the random points into a curve using a polynomial solution (second to eighth order), resulting in 1 million possible sea-level scenarios.

iv. Initial Cliff Inclination (ICI) and v. Measured Notch Profiles (MNP): A randomly selected MNP determined the initial cliff plane for notch formation modeling from 22 profiles obtained via SfM-MVS (Figure 1a-v). Three inclinations were derived from the chosen MNP (Figure 1a-iv): minimum (min) (hypotenuse across notch's roof and floor), vertical (90°-max), and median (med). The final fitting inclination was randomly chosen from min, med, or 90° options. Slope values derived from cliff mapping ranged from 60 to 90°.

2.3. Sea Level Curves Clustering

To assess the simulation outcomes and differentiate the modeled SLCs, we devised a clustering protocol that categorizes the most congruent SLCs according to their complexity. Since our model cannot discern between an early and a late sea-level rise (i.e.,: mirrored sea-level curves yield identical results, leading to the development of the same notch geometry) for each ER (0.25–2 mm/a) (Figure S2a in Supporting Information S1) we first used the Linear Regression statistical method to discriminate the SLCs based on their slope (positive (+) to negative (−), Figure S2b in Supporting Information S1). Subsequently, for every group identified, subgroups were formed based on the number of peaks present in each curve, categorizing the SLC types as single rise, 1 peak, 2 peaks, 3 peaks, or more than 3 peaks (Figure S2c in Supporting Information S1). While the sea level curve shapes for the scenarios involving "1 peak" to "3 or more peaks" are easily understandable, the single rise scenario spans the entire duration given and requires its post-peak decline to exceed the erosion rate, ensuring that the notch geometry remains unaltered while sea level is dropping. Conversely, in the "1 peak" scenario, the rate of sea level drop has the capacity to reshape the geometry of the notch. Finally, in each of these subgroups, the *K-means* unsupervised clustering algorithm (Lloyd, 1982) was employed (Figure S2d in Supporting Information S1). *K-means* clustering is an iterative algorithm that partitions a dataset into k distinct, non-overlapping clusters based on their similarities, aiming to minimize the variance within each cluster. The algorithm underwent multiple manual iterations, adjusting the number of clusters, to ascertain the optimal clustering outcome (best-fitting cluster). The best-fitting clusters as well as their scores are presented in Table S1 in Supporting Information S1.

3. Results

3.1. Tidal Notch Background and Morphometry

The Orosei Gulf's relic tidal notch, stretching 70 km (Figure 2), represents a globally significant example of LIG sea level action (Antonioli et al., 2006, 2018; Antonioli & Ferranti, 1992) on a Jurassic 300 m high carbonate cliff (D'Angeli et al., 2015). Its exceptional preservation is attributed to its burial by continental talus, protecting it from erosion (Antonioli & Ferranti, 1992). Its formation is linked to isostatic subsidence during the LIG (Antonioli et al., 2006). Despite Sardinia's tectonic stability (Vacchi et al., 2018), MIS5e SLIPs in the Orosei Gulf show unusual elevation differences (+9.5 m compared to +3.5–6 m amsl, Figure 2e), suggesting that magmatic intrusion uplifted the area by 2.4 ± 0.2 m (Mariani et al., 2009), contrasting with lower elevations in the West Sardinia attributed to continental margin downthrow or fault related subsidence. Mariani et al. (2009) applied various loads in an isostatic flexure model, independent of Last Interglacial shoreline elevations, thereby avoiding any circularity. Presumably, the magmatic intrusion occurred after the notch formation, since volcanic deposits

19448007, 2024, 6, Downloaded from https://agupubs.onlinelibrary.wiley.com/doi/10.1029/2023GL106829 by CochraneItalia, Wiley Online Library on [19/03/2024]. See the Terms and Conditions (https://onlinelibrary.wiley.com/terms-and-conditions) on Wiley Online Library for rules of use; OA articles are governed by the applicable Creative Commons License

younger than 125 ka BP were found filling MIS 5e lithophaga boreholes (Antonioli et al., 2006). Moreover, the uplifting factor further enhances the remarkable preservation observed in this case, since uplifted areas tend to preserve SLIPs in a better condition (Georgiou et al., 2022; Mattei et al., 2022; Pedoja et al., 2014). The Orosei notch geometry departs from the classic single parabolic indentation, displaying a "double notch" morphology (Figures 2c and 2d) as described by Antonioli et al. (2006).

3.2. Best-Fitting Sea-Level Curves

We simulated the shape of the Orosei notch by exploring 1 million combinations of the variables, as elaborated in the methodology (Figure 1). Results with a high fit (≥80%) to the MNPs can be achieved by any scenario of initial cliff inclination. Instead, it was not possible to obtain high fit results using ERs akin to current ones (0.25 mm/a) (Table S1 in Supporting Information S1). To accurately represent the measured notch geometry, we had to impose a greater than modern ER (higher than 0.5 mm/a), which allowed obtaining a fit between modeled and measured notch profiles exceeding 80% (see Supporting Information for details, Table S1 in Supporting Information S1). In general, our results show that, as the complexity of SLCs increases, the fit of the modeled results with MNPs diminishes. The optimal average fit (83.8%) was obtained with an ER of 1 mm/a combined with the lowest SLC complexity (single rise). The same cluster yielded the overall best-fitting score of 91.6%. Notably, the second-best fit (90.1%) was produced when employing the 2 mm/a ER scenario and under a 2-peak sea level scenario. However, the complexity of the SLC was irrelevant to the efficiency of the model under the highest ER scenario (2 mm/a) since both the lowest and highest complexity equally fitted the measured notch (83.3%).

Probability density plots of the sea level distribution (Figure 3) were constructed for each cluster shown in Table S1 in Supporting Information S1. The distribution of the sea level (y-axis) is shown over a period of 15 ka (x-axis), providing an insight into the sea-level variability during the LIG. The plots were weighted based on their fitting score, normalized from 0 to 1, and are described as low to high confidence distributions respectively.

The findings indicate that an ER of 0.5 mm/a, the closest to modern ERs, can effectively replicate the observed notch morphology (82.5%) only under the "single rise" complexity scenario. In this scenario, the sea level rise rates vary between 0.3 and 0.8 mm/a, and the peak sea level is reached at 5.5 ± 1 m. Fitting scores are significantly improving while increasing the ER (1 mm/a–91.6% fitting) with sea level fluctuating more rapidly (0.5–1 mm/a).

The morphology of the Orosei notch could be replicated by the model also under a double-peak sea level scenario (maximum fitting of 90.1%), but only quadrupling the ER (2 mm/a). In such cases, SLCs are characterized by a quick initial SLR rate (3.5–6 mm/a) followed by a short-lived sea level peak at 3.5–4 ± 1 m. Shortly after, sea level drops to an elevation of 1 m at a rate lower than 2 mm/a. Then, the sea level reaches a second peak through a relatively rapid sea level rise (1.5 mm/a), reaching a second peak at 6 m above modern sea level.

The same ER (2 mm/a) effectively replicated the measured notch morphology for increased complexity SLCs (3 peaks). These SLCs show three distinct peaks at levels of about 4, 5, and 6 ± 1 m. Scenarios of even higher complexity, involving four peaks, diminish the efficacy of the simulations to a maximum of 88.8%, concurrently lowering the reliability of our sea level distributions.

4. Discussion

4.1. Simulated and Predicted Sea-Level Variability

The LIG vertical land movements in the Orosei Gulf were primarily modulated by the isostatic crustal response to surface loadings and secondarily by low-magnitude tectonic drivers that occurred after the development of the notch. During the late phase of the LIG, the Central-Western Mediterranean and Sardinian coasts experienced isostatic subsidence due to water loading in the Tyrrhenian Sea (Lambeck et al., 2004; Stocchi et al., 2018), which is likely the primary cause of regional sea level rise and the enlarged geometry of the notch (Antonioli et al., 2006). By eliminating the post-uplifting factor (2.4 m ± 0.2, see Section 3.1), the sea level probability density distribution reveals that the combined contributions of eustatic and isostatic processes confidently yield a maximum paleo RSL value of 6 ± 0.2 m (Figure 3). This outcome remains consistent throughout all the model simulations irrespective of the variables utilized in constructing the SLCs. To add to this, this elevation aligns with the measured MIS5e RSL indicators surrounding the island of Sardinia (Figure 2e).

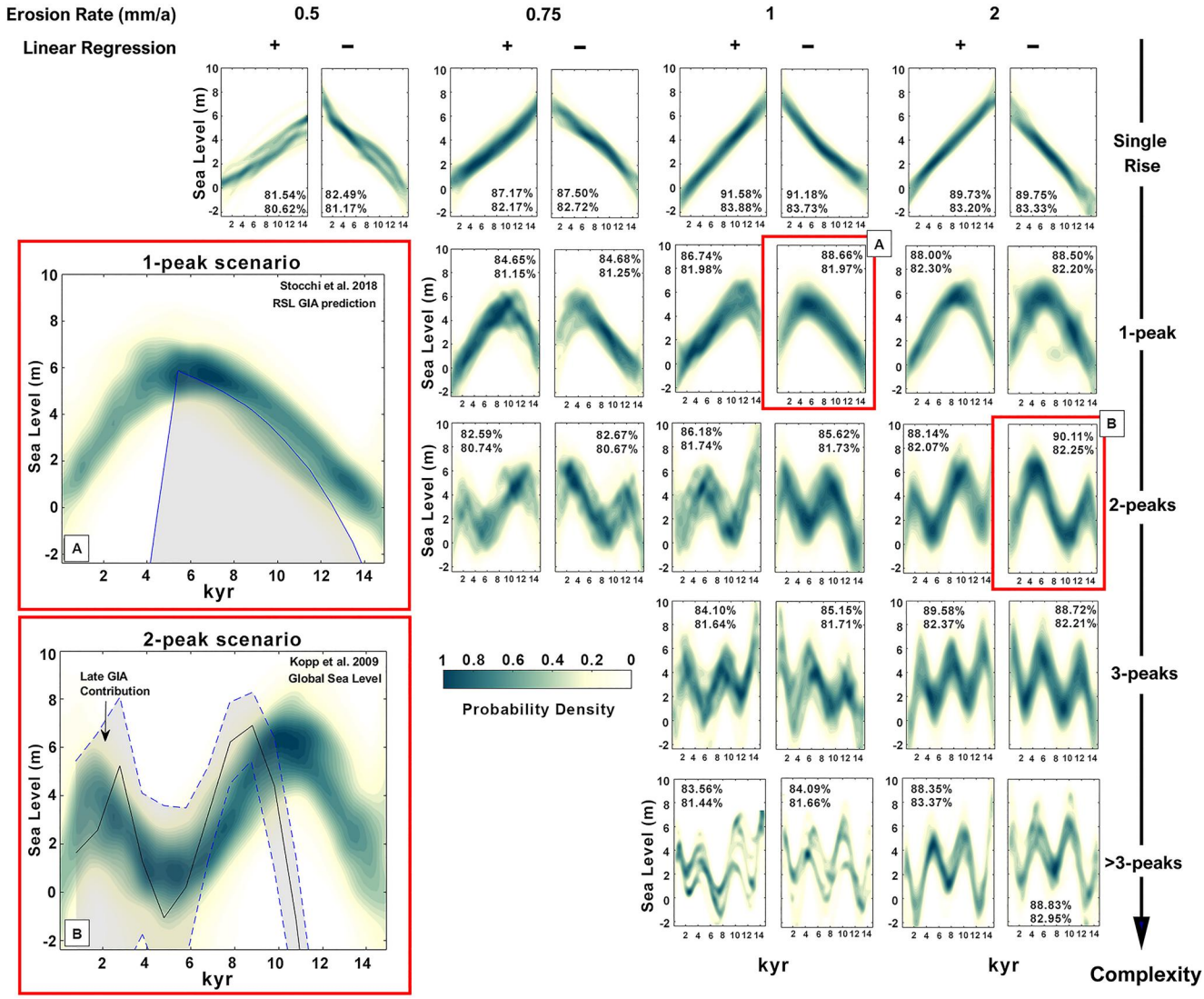

Figure 3. Probability density plots exhibit the distribution of best-fitting sea level clusters (Table S1 in Supporting Information S1). Plots are grouped based on the Erosion Rate (0.5–2 mm/a) and the Linear Regression (positive-negative), while the SLCs complexity is increasing vertically (single rise, 1-peak,…, >3-peaks). Figure 3. (a) and (b) Simulated sea-level probability density plots in comparison to (a) relative sea level (RSL) prediction based on GIA model from Stocchi et al. (2018), (concurrent melting of the Greenland Ice Sheet (GrIS) and Antarctic Ice Sheet (AIS)), (b) probabilistic sea-level of Kopp et al. (2009), highlighting the asynchronous melting of the GrIS and AIS, coupled with the GIA subsidence during the later phase of the LIG (Data available in Georgiou (2023b), https://doi.org/10.5281/zenodo.8407819).

Our best-fitting simulated SLCs were those exhibiting a single highstand peak scenario (complexity: single rise or 1 peak – ER: 1–2 mm/a), yet good-fitting results were obtained through the 0.5 mm/a ER scenario, which is more consistent with present-day ERs. These SLCs align closely with those predicted by the GIA models of Stocchi et al. (2018) for SE Sardinia, which model the simultaneous GrIS and AIS melting early in the interglacial (Figure 3a). Our results are further reinforced by Antonioli et al. (2006) who surmised that the morphometry of the notch was merely attributed to late LIG isostatic subsidence, a process which is believed to have been reactivated during the MIS 1 (Vacchi et al., 2018). A one-peak scenario is also in agreement with the absence of sea-level fluctuations during the LIG suggested by Barlow et al. (2018). This result endorses the efficiency of our methodology for reconstructing the regional RSL based on the geometry of a tidal notch.

A double-peak scenario showed exceptional fitting under an enhanced erosion rate scenario with two sea level peaks at 4 and 6 ± 1 m separated by a sea level drop close to 1 m. The sea level distribution aligns closely with the global sea level range as predicted by Kopp et al. (2009). This would support the asynchronous ice sheet

19448007, 2024, 6, Downloaded from https://agupubs.onlinelibrary.wiley.com/doi/10.1029/2023GL106829 by CochraneItalia, Wiley Online Library on [19/03/2024]. See the Terms and Conditions (https://onlinelibrary.wiley.com/terms-and-conditions) on Wiley Online Library for rules of use; OA articles are governed by the applicable Creative Commons License

19448007, 2024, 6, Downloaded from https://agupubs.onlinelibrary.wiley.com/doi/10.1029/2023GL106829 by CochraneItalia, Wiley Online Library on [19/03/2024]. See the Terms and Conditions (https://onlinelibrary.wiley.com/terms-and-conditions) on Wiley Online Library for rules of use; OA articles are governed by the applicable Creative Commons License

melting scenario with an early contribution of the AIS, followed by a lowstand below modern sea level and a late simultaneous contribution of GrIS and AIS (Dumitru et al., 2023; Rohling et al., 2019). During the later phase of the LIG, glacial-isostatic subsidence of eastern Sardinia possibly co-contributed to the RSL rise (Figure 3b). Relative SLIPs identified in the Western Mediterranean suggest that a double eustatic highstand scenario could bridge the differences between the predicted paleo RSL and observed superimposed fossil beach deposits (Hearty et al., 2007; Lorscheid, Felis, et al., 2017; Lorscheid, Stocchi, et al., 2017). This is consistent with trends outlined in coral records (O'Leary et al., 2013; Thompson & Goldstein, 2005), corroborated by paleoceanographic evidence (Grant et al., 2012; Rohling et al., 2019). This aids in understanding the time-varying impacts of the GrIS and AIS and illuminates the WAIS collapse which occurred under milder climatic forcing (Lau et al., 2023).

Finally, a rapidly fluctuating triple SL peak structure (Figure 3) aligns closely with the probabilistic approach produced from the continuous indirect sea-level record of the KL11-KL23 Red Sea sediment cores (Grant et al., 2012; Rohling et al., 2019). Although it is a plausible scenario, it remains to be supported through direct proxies since past abrupt sea level fluctuations may have left scarce direct traces, except for a triple reef structure in the Red Sea (Bruggemann et al., 2004).

Carobene (2015) documented four LIG highstands from bioerosional grooves in Orosei sea caves. Multiple highstands imply rapid sea level rise and meltwater input, suggesting likely future extreme sea-level rise under a warmer climate (Silvano et al., 2018; Rholing et al., 2019).

Overall, our findings indicate that the sea level during the LIG reached a maximum peak of 6 ± 1 m, which lies in the upper range of the estimate by Dyer et al. (2021), who assert a mere 5% likelihood of the sea level exceeding 5.3 m.

4.2. Tidal Notch Formation Mechanisms During the Last Interglacial (LIG)

Along the Mediterranean, limestone ERs have been reported to vary between 0.1 and 2 mm/a (Antonioli et al., 2015; Boulton & Stewart, 2015; Evelpidou & Pirazzoli, 2016; Furlani & Cucchi, 2013; Furlani et al., 2014; Karkani & Evelpidou, 2021; Pirazzoli & Evelpidou, 2013). Given the relative stability of the sea level in the last 3–4 ka, it's proposed that East Sardinia's limestones have an ER of 0.25–0.33 mm/a, as observed from modern tidal notch measurements (Antonioli et al., 2018; Vacchi et al., 2021). Our numerical model effectively replicated the observed notch using a minimum cumulative ER of 0.5 mm/a, which is slightly higher than the modern one reported above. It should be noted that by increasing the complexity of the sea level curvature, only higher ERs were accomplishing the replication of the notch geometry.

Abrasion of the notch due to the presence of a sand beach was previously excluded (Antonioli et al., 2006), therefore one justification for the mismatch between the ER giving us the best results and measured ERs may reside in the fact that ERs could have been regionally increased, during the LIG, due to enhanced chemical dissolution from karst freshwater supply (Antonioli et al., 2006), greater bioerosion (Mottershead, 2013) or increased wave energy (Sunamura, 2019). Even if wave dynamics during the LIG period remain a complex subject of scientific inquiry, recent studies showed that warmer climate phases can affect both wave circulation patterns (Goodwin et al., 2023) and storm wave energy (Reguero et al., 2019; Wolf et al., 2020) thereby intensifying erosional processes and exerting significant mechanical force upon coastlines. Under these assumptions, our model results suggest that the tidal notch is indeed an MIS 5e relict (Antonioli et al., 2006) since it can be developed with a slightly higher ER compared to the present one (but included in the present ER range of 0.1–2 mm/a) and there is no need to invoke the effect of overprinting or reoccupation upon a previous sea-level highstand as detected in other study areas (De Santis et al., 2023; Pastier et al., 2019).

While karst dissolution may have increased the erosion rate, the notch's remarkable preservation due to burial during MIS 4-2 (Antonioli & Ferranti, 1992), in conjunction with precise morphometric analysis (Text S2 and Figure S1 in Supporting Information S1), effectively isolated the intact segments for accurate model representation.

The initial cliff plane significantly influences notch geometry. Various initial cliff inclinations (60°–85° and 85°–90°) result in diverse notch shapes under uniform sea level changes. This confirms that notch asymmetries are linked to the initial cliff inclination (ICI) where the notch originated (Trenhaile, 2016), indicating that lower ICIs extend the notch floor.

19448007, 2024, 6, Downloaded from https://agupubs.onlinelibrary.wiley.com/doi/10.1029/2023GL106829 by CochraneItalia, Wiley Online Library on [19/03/2024]. See the Terms and Conditions (https://onlinelibrary.wiley.com/terms-and-conditions) on Wiley Online Library for rules of use; OA articles are governed by the applicable Creative Commons License

5. Conclusions

In this study, we employed a simple numerical model to simulate the morphology of one of the best-preserved tidal notches dated to the LIG, in an attempt to reverse the classic workflow used to study past changes in sea level and derive, from a single sea-level indicator, a suitable set of sea level curves that can explain its morphology. While there are caveats to our modeling (discussed above), our results allow us to draw several conclusions.

1. Limestone erosion rates at our site might have been higher in the LIG. This follows from the fact that using modern erosion rates, our model has a low success rate in replicating the observed notch morphology under any combination of the other variables.
2. The highest fit between modeled and observed notch morphology is obtained with a LIG sea-level history characterized by a single sea-level peak. In this scenario, the sea-level history (in particular, the RSL rise rate) seems to coincide very well with RSL as reproduced by GIA models.
3. Using higher limestone erosion rates, our model can reproduce the notch profile under more complex LIG sea-level scenarios (2-peak, 3-peak or more), similar to those reported in the literature, suggesting rapid sea level rise during the LIG.
4. Under any model, we can reproduce the modern morphology of the notch by considering a slight post-tectonic uplift since the LIG. The peak sea level reached in any scenario is close to 6 m above present, which in our case would be the sum of eustatic (ice equivalent) sea level and post-depositional effects other than tectonics (i.e., GIA).

Data Availability Statement

The scripts used for the numerical model and the figure production are made available in the open platform GitHub, archived in the Zenodo repository licensed under MIT License, and can be cited as Georgiou (2023a). The results produced are publicly available and archived in Zenodo, Georgiou (2023b), licensed under Creative Commons Attribution 4.0 International.

Acknowledgments
This work was funded by the European Research Council (ERC) under the European Union's Horizon 2020 research and innovation program (Grant Agreement n. 802414- WARMCOASTS). We acknowledge the Erasmus + Traineeship Mobility Agreement (ID 2649) and the PALSEA, a working group of the International Union for Quaternary Sciences (INQUA).

References

Antonioli, F., Ferranti, L., & Kershaw, S. (2006). A glacial isostatic adjustment origin for double MIS 5.5 and Holocene marine notches in the coastline of Italy. *Quaternary International*, *145–146*, 19–29. https://doi.org/10.1016/j.quaint.2005.07.004

Antonioli, F., Lo Presti, V., Rovere, A., Ferranti, L., Anzidei, M., Furlani, S., et al. (2015). Tidal notches in Mediterranean Sea: A comprehensive analysis. *Quaternary Science Reviews*, *119*, 66–84. https://doi.org/10.1016/J.QUASCIREV.2015.03.016

Antonioli, & Ferranti, L. (1992). Geomorfologia costiera e subacquea e considerazioni paleoclimatiche sul settore compreso tra S. Maria Navarrese e Punta Goloritzé (Golfo di Orosei, Sardegna). *Giornale di Geologia*, *54*(2), 66–89.

Antonioli, Ferranti, L., Stocchi, P., Deiana, G., Lo Presti, V., Furlani, S., et al. (2018). Morphometry and elevation of the last interglacial tidal notches in tectonically stable coasts of the Mediterranean Sea. *Earth-Science Reviews*, *185*, 600–623. Elsevier B.V. https://doi.org/10.1016/j.earscirev.2018.06.017

Barlow, N. L. M., McClymont, E. L., Whitehouse, P. L., Stokes, C. R., Jamieson, S. S. R., Woodroffe, S. A., et al. (2018). Lack of evidence for a substantial sea-level fluctuation within the Last Interglacial. *Nature Geoscience*, *11*(9), 627–634. https://doi.org/10.1038/s41561-018-0195-4

Belluomini, G., Branca, M., Delitala, L., Pecorini, G., & Spano, C. (1986). Isoleucine epimerization dating of Quaternary marine deposits in Sardinia, Italy in Dating Mediterranean shorelines. *Zeitschrift für Geomorphologie*, *62*, 109–117.

Boulton, S. J., & Stewart, I. S. (2015). Holocene coastal notches in the Mediterranean region: Indicators of palaeoseismic clustering? *Geomorphology*, *237*, 29–37. https://doi.org/10.1016/j.geomorph.2013.11.012

Bruggemann, J. H., Buffler, R. T., Guillaume, M. M. M., Walter, R. C., Von Cosel, R., Ghebretensae, B. N., & Bertie, S. M. (2004). Stratigraphy, palaeoenvironments and model for the deposition of the Abdur Reef Limestone: Context for an important archaeological site from the last interglacial on the Red Sea coast of Eritrea. *Palaeogeography, Palaeoclimatology, Palaeoecology*, *203*(3–4), 179–206. https://doi.org/10.1016/S0031

Carobene, L. (2015). Marine notches and sea-cave bioerosional grooves in microtidal areas: Examples from the Tyrrhenian and Ligurian Coasts—Italy. *Journal of Coastal Research*, *31*(3), 536–556. https://doi.org/10.2112/JCOASTRES-D-14-00068.1

Carrivick, M. W. S., & Quincey, D. J. (2016). Structure from motion in the GeoSciences. Retrieved from https://onlinelibrary.wiley.com/doi/

Casella, E., Rovere, A., Pedroncini, A., Stark, C. P., Casella, M., Ferrari, M., & Firpo, M. (2016). Drones as tools for monitoring beach topography changes in the Ligurian Sea (NW Mediterranean). *Geo-Marine Letters*, *36*(2), 151–163. https://doi.org/10.1007/s00367-016-0435-9

Cerrone, C., Vacchi, M., Fontana, A., & Rovere, A. (2021). Last Interglacial sea-level proxies in the western Mediterranean. *Earth System Science Data*, *13*(9), 4485–4527. https://doi.org/10.5194/essd-13-4485-2021

Chutcharavan, P. M., & Dutton, A. (2021). A global compilation of U-series-dated fossil coral sea-level indicators for the Last Interglacial period (Marine Isotope Stage 5e). *Earth System Science Data*, *13*(7), 3155–3178. https://doi.org/10.5194/essd-13-3155-2021

D'Angeli, I. M., Sanna, L., Calzoni, C., & De Waele, J. (2015). Uplifted flank margin caves in telogenetic limestones in the Gulf of Orosei (Central-East Sardinia-Italy) and their palaeogeographic significance. *Geomorphology*, *231*, 202–211. https://doi.org/10.1016/j.geomorph.2014.12.008

De Santis, V., Scardino, G., Scicchitano, G., Meschis, M., Montagna, P., Pons-Branchu, E., et al. (2023). Middle-late Pleistocene chronology of palaeoshorelines and uplift history in the low-rising to stable Apulian foreland: Overprinting and reoccupation. *Geomorphology*, *421*, 108530. https://doi.org/10.1016/j.geomorph.2022.108530

Dumitru, O. A., Dyer, B., Austermann, J., Sandstrom, M. R., Goldstein, S. L., D'Andrea, W. J., et al. (2023). Last interglacial global mean sea level from high-precision U-series ages of Bahamian fossil coral reefs. *Quaternary Science Reviews*, *318*, 108287. https://doi.org/10.1016/j.quascirev.2023.108287

Dutton, A., Webster, J. M., Zwartz, D., Lambeck, K., & Wohlfarth, B. (2015). Tropical tales of polar ice: Evidence of Last Interglacial polar ice sheet retreat recorded by fossil reefs of the granitic Seychelles islands. *Quaternary Science Reviews*, *107*, 182e196–196. https://doi.org/10.1016/j.quascirev.2014.10.025

Dyer, B., Austermann, J., D'Andrea, W. J., Creel, R. C., Sandstrom, M. R., Cashman, M., et al. (2021). Sea-level trends across the Bahamas constrain peak last interglacial ice melt. *P. Natl. Acad. Sci. USA*, *118*(33), e2026839118. https://doi.org/10.1073/pnas.2026839118

Eckhardt, R. (1987). Stan Ulam, John von Neumann,and the Monte Carlo method. *Los Alamos Sci.Spec. Issue*, *15*, 131–137.

Evelpidou, N., & Pirazzoli, P. A. (2016). Estimation of the intertidal bioerosion rate from a well-dated fossil tidal notch in Greece. *Marine Geology*, *380*, 191–195. https://doi.org/10.1016/J.MARGEO.2016.04.017

Evelpidou, N., Pirazzoli, P. A., Saliège, J. F., & Vassilopoulos, A. (2011). Submerged notches and doline sediments as evidence for Holocene subsidence. *Continental Shelf Research*, *31*(12), 1273–1281. https://doi.org/10.1016/j.csr.2011.05.002

Evelpidou, N., Vassilopoulos, A., & Pirazzoli, P. A. (2012). Submerged notches on the coast of Skyros Island (Greece) as evidence for Holocene subsidence. *Geomorphology*, *141–142*, 81–87. https://doi.org/10.1016/j.geomorph.2011.12.025

Florinsky, I. V. (2017). An illustrated introduction to general geomorphometry. *Progress in Physical Geography: Earth and Environment*, *41*(6), 723–752. https://doi.org/10.1177/0309133317733667

Furlani, S., & Cucchi, F. (2013). Downwearing rates of vertical limestone surfaces in the intertidal zone (Gulf of Trieste, Italy). *Marine Geology*, *343*, 92–98. https://doi.org/10.1016/J.MARGEO.2013.06.005

Furlani, S., Ninfo, A., Zavagno, E., Paganini, P., Zini, L., Biolchi, S., et al. (2014). Submerged notches in Istria and the Gulf of Trieste: Results from the Geoswim project. *Quaternary International*, *332*, 37–47. https://doi.org/10.1016/j.quaint.2014.01.018

Georgiou, N. (2023a). Nikos-Georgiou/TidalNotch_Generator_v1: TidalNotch generator v1.0.0 (TidalNotchv1.0.0). *Zenodo*. [Software]. https://doi.org/10.5281/zenodo.8407427

Georgiou, N. (2023b). Best-fitting Sea Level Curves generated from TidalNotch Generator model (v1.0.0). [Dataset]. *Zenodo*. https://doi.org/10.5281/zenodo.8407819

Georgiou, N., Geraga, M., Francis-Allouche, M., Christodoulou, D., Stocchi, P., Fakiris, E., et al. (2022). Late Pleistocene submarine terraces in the Eastern Mediterranean, central Lebanon, Byblos: Revealing their formation time frame through modeling. *Quaternary International*, *638–639*, 180–196. https://doi.org/10.1016/j.quaint.2021.12.008

Georgiou, N., Rovere, A., Stocchi, P., & Casella, E. (2020). Reconstructing past sea level through notches: Orosei Gulf. In *IMEKO TC-19 International Workshop on Metrology for the Sea*. Retrieved from https://www.imeko.org/publications/tc19-Metrosea-2020/IMEKO-TC19-MetroSea-2020-35.pdf

Goodwin, I. D., Mortlock, T. R., Ribo, M., Mitrovica, J. X., O' Leary, M., & Williams, R. (2023). Robbins Island: The index site for regional Last Interglacial sea level, wave climate and the subtropical ridge around Bass Strait, Australia. *Quaternary Science Reviews*, *305*, 107996. https://doi.org/10.1016/j.quascirev.2023.107996

Grant, K. M., Rohling, E. J., Bar-Matthews, M., Ayalon, A., Medina-Elizalde, M., Ramsey, C. B., et al. (2012). Rapid coupling between ice volume and polar temperature over the past 150,000 years. *Nature*, *491*(7426), 744–747. https://doi.org/10.1038/nature11593

Hearty, P. J. (1986). An inventory of last interglacial (sensu lato) age deposits from the Mediterranean basin: A study of isoleucine epimerization and U- series dating. *Zeitschrift für Geomorphologie*, *62*, 51–69.

Hearty, P. J., Hollin, J. T., Neumann, A. C., O'Leary, M. J., & McCulloch, M. (2007). Global sea-level fluctuations during the Last Interglaciation (MIS 5e). *Quaternary Science Reviews*, *26*(17–18), 2090–2112. https://doi.org/10.1016/j.quascirev.2007.06.019

Horn, B. K. P. (1981). Hill shading and the reflectance map. *Proceedings of the IEEE*, *69*(1), 14–47. https://doi.org/10.1109/PROC.1981.11918

Karkani, A., & Evelpidou, N. (2021). Multiple submerged tidal notches: A witness of sequences of coseismic subsidence in the Aegean Sea, Greece. *Journal of Marine Science and Engineering*, *9*(4), 426. https://doi.org/10.3390/jmse9040426

Kopp, R. E., Simons, F. J., Mitrovica, J. X., Maloof, A. C., & Oppenheimer, M. (2009). Probabilistic assessment of sea level during the last interglacial stage. *Nature*, *462*(7275), 863–867. https://doi.org/10.1038/nature08686

Lambeck, K., Antonioli, F., Purcell, A., & Silenzi, S. (2004). Sea-level change along the Italian coast for the past 10,000 yr. *Quaternary Science Reviews*, *23*(14–15), 1567–1598. https://doi.org/10.1016/j.quascirev.2004.02.009

Larson, M. P., Sunamura, T., Erikson, L., Bayram, A., & Hanson, H. (2010). An analytical model to predict dune and cliff notching due to wave impact. *Coastal Engineering Proceedings*, *1*(32), 35. sediment.35. https://doi.org/10.9753/icce.v32.sediment.35

Lau, S. C. Y., Wilson, N. G., Golledge, N. R., Naish, T. R., Watts, P. C., Silva, C. N. S., et al. (2023). Genomic evidence for West Antarctic Ice Sheet collapse during the Last Interglacial. *Science*, *382*(6677), 1384–1389. https://doi.org/10.1126/science.ade0664

Lloyd, S. (1982). Least squares quantization in PCM. *IEEE Transactions on Information Theory*, *28*(2), 129–137. https://doi.org/10.1109/TIT.1982.1056489

Lorscheid, T., Felis, T., Stocchi, P., Obert, J. C., Scholz, D., & Rovere, A. (2017). Tides in the last interglacial: Insights from notch geometry and palaeo tidal models in Bonaire, Netherland Antilles. *Scientific Reports*, *7*(1), 16241. https://doi.org/10.1038/s41598-017-16285-6

Lorscheid, T., Stocchi, P., Casella, E., Gómez-Pujol, L., Vacchi, M., Mann, T., & Rovere, A. (2017). Paleo sea-level changes and relative sea-level indicators: Precise measurements, indicative meaning and glacial isostatic adjustment perspectives from Mallorca (Western Mediterranean). *Palaeogeography, Palaeoclimatology, Palaeoecology*, *473*, 94–107. https://doi.org/10.1016/j.palaeo.2017.02.028

Mariani, P., Braitenberg, C., & Antonioli, F. (2009). Sardinia coastal uplift and volcanism. *Pure and Applied Geophysics*, *166*(8–9), 1369–1402. https://doi.org/10.1007/s00024-009-0504-3

Mattei, G., Caporizzo, C., Corrado, G., Vacchi, M., Stocchi, P., Pappone, G., et al. (2022). On the influence of vertical ground movements on Late-Quaternary sea-level records. A comprehensive assessment along the mid-Tyrrhenian coast of Italy (Mediterranean Sea). *Quaternary Science Reviews*, *279*, 107384. https://doi.org/10.1016/j.quascirev.2022.107384

Mottershead, D. (2013). 4.13 Coastal weathering. *Treatise on Geomorphology*, *1–14*(1–14), 228–244. https://doi.org/10.1016/B978-0-12-374739-6.00064-6

Olaya, V. (2009). *Chapter 6 basic land-surface parameters*. In T. Hengl & H. I. Reuter (Eds.), *Developments in soil science* (Vol. 33, pp. 141–169). Elsevier. https://doi.org/10.1016/S0166-2481(08)00006-8

O'Leary, M. J., Hearty, P. J., Thompson, W. G., Raymo, M. E., Mitrovica, J. X., & Webster, J. M. (2013). Ice sheet collapse following a prolonged period of stable sea level during the last interglacial. *Nature Geoscience*, *6*(9), 796–800. https://doi.org/10.1038/ngeo1890

19448007, 2024, 6, Downloaded from https://agupubs.onlinelibrary.wiley.com/doi/10.1029/2023GL106829 by CochraneItalia, Wiley Online Library on [19/03/2024]. See the Terms and Conditions (https://onlinelibrary.wiley.com/terms-and-conditions) on Wiley Online Library for rules of use; OA articles are governed by the applicable Creative Commons License

Pastier, A.-M., Husson, L., Pedoja, K., Bézos, A., Authemayou, C., Arias-Ruiz, C., & Cahyarini, S. Y. (2019). Genesis and architecture of sequences of quaternary coral reef terraces: Insights from numerical models. *Geochemistry, Geophysics, Geosystems*, *20*(8), 4248–4272. https://doi.org/10.1029/2019GC008239

Pedoja, K., Husson, L., Johnson, M. E., Melnick, D., Witt, C., Pochat, S., et al. (2014). Coastal staircase sequences reflecting sea-level oscillations and tectonic uplift during the Quaternary and Neogene. *Earth-Science Reviews*, *132*, 13–38. https://doi.org/10.1016/j.earscirev.2014.01.007

Pirazzoli (1986). Marine notches. In *Sea-Level Research: A Manual for the Collection and Evaluation of Data*.

Pirazzoli, P., Laborel, J., Saliège, J. F., Erol, O., Kayan, İ., & Person, A. (1991). Holocene raised shorelines on the Hatay coasts (Turkey): Palaeoecological and tectonic implications. *Marine Geology*, *96*(3), 295–311. https://doi.org/10.1016/0025-3227(91)90153-U

Pirazzoli, P. A. (2005). A review of possible eustatic, isostatic and tectonic contributions in eight late-Holocene relative sea-level histories from the Mediterranean area. *Quaternary Science Reviews*, *24*(18–19), 1989–2001. https://doi.org/10.1016/J.QUASCIREV.2004.06.026

Pirazzoli, P. A., & Evelpidou, N. (2013). Tidal notches: a seasea-level indicator of uncertain archival trustworthiness. *Palaeogeography, Palaeoclimatology, Palaeoecology*, *369*, 377–384. https://doi.org/10.1016/j.palaeo.2012.11.004

Polyak, V. J., Onac, B. P., Fornós, J. J., Hay, C., Asmerom, Y., Dorale, J. A., et al. (2018). A highly resolved record of relative sea level in the western Mediterranean Sea during the last interglacial period. *Nature Geoscience*, *11*(11), 860–864. https://doi.org/10.1038/s41561-018-0222-5

Reguero, B. G., Losada, I. J., & Méndez, F. J. (2019). A recent increase in global wave power as a consequence of oceanic warming. *Nature Communications*, *10*(1), 205. https://doi.org/10.1038/s41467-018-08066-0

Rohling, E. J., Grant, K., Hemleben, C., Siddall, M., Hoogakker, B. A. A., Bolshaw, M., & Kucera, M. (2008). High rates of sea-level rise during the last interglacial period. *Nature Geoscience*, *1*(1), 38–42. https://doi.org/10.1038/ngeo.2007.28

Rohling, E. J., Hibbert, F. D., Grant, K. M., Galaasen, E. V., Irvalı, N., Kleiven, H. F., et al. (2019). Asynchronous Antarctic and Greenland ice-volume contributions to the last interglacial sea-level highstand. *Nature Communications*, *10*(1), 5040. https://doi.org/10.1038/s41467-019-12874-3

Rovere, A., Ryan, D. D., Vacchi, M., Dutton, A., Simms, A. R., & Murray-Wallace, C. V. (2023). The World Atlas of last interglacial shorelines (version 1.0). *Earth System Science Data*, *15*(1), 1–23. https://doi.org/10.5194/essd-15-1-2023

Sappington, J. M., Longshore, K. M., & Thompson, D. B. (2007). Quantifying landscape ruggedness for animal habitat analysis: A case study using Bighorn Sheep in the Mojave Desert. *Journal of Wildlife Management*, *71*(5), 1419–1426. https://doi.org/10.2193/2005-723

Schneiderwind, S., Boulton, S. J., Papanikolaou, I., Kázmér, M., & Reicherter, K. (2017). Numerical modeling of tidal notch sequences on rocky coasts of the Mediterranean Basin. *Journal of Geophysical Research: Earth Surface*, *122*(5), 1154–1181. https://doi.org/10.1002/2016JF004132

Shennan, I. (2015). Handbook of sea-level research. In *Handbook of Sea-Level Research* (pp. 3–25). https://doi.org/10.1002/9781118452547.ch2

Silvano, A., Rintoul, S. R., Peña-Molino, B., Hobbs, W. R., Wijk, E., Aoki, S., et al. (2018). Freshening by glacial meltwater enhances melting of ice shelves and reduces formation of Antarctic Bottom Water. *Science Advances*, *4*. eaap9467(2018). https://doi.org/10.1126/sciadv.aap9467

Stocchi, P., Vacchi, M., de Boer, B., Lorscheid, T., Simms, A. R., vande Wal, R. S. W., et al. (2018). MIS 5e relative sea-level changes in the Mediterranean Sea: Contribution of isostatic disequilibrium. *Quaternary Science Reviews*, *185*, 122–134. https://doi.org/10.1016/j.quascirev.2018.01.004

Sunamura, T. (2019). *Cliffs, erosion rates*. In C. W. Finkl & C. Makowski (Eds.), *Encyclopedia of coastal science* (pp. 398–403). Springer International Publishing. https://doi.org/10.1007/978-3-319-93806-6_71

Thompson, W. G., & Goldstein, S. L. (2005). Open-system coral ages reveal persistent suborbital sea-level cycles. *Science*, *308*(5720), 401–404. https://doi.org/10.1126/science.1104035

Trenhaile, A. (2016). Modelling coastal notch morphology and developmental history in the Mediterranean. *GeoResJ*, *9–12*, 77–90. https://doi.org/10.1016/j.grj.2016.09.003

Trenhaile, A. S. (2001). Modeling the effect of late Quaternary interglacial sea levels on wave-cut shore platforms. *Marine Geology*, *172*(3–4), 205–223. https://doi.org/10.1016/s0025-3227(00)00136-5

Trenhaile, A. S. (2014). Modelling tidal notch formation by wetting and drying and salt weathering. *Geomorphology*, *224*, 139–151. https://doi.org/10.1016/j.geomorph.2014.07.014

Trenhaile, A. S. (2015). Coastal notches: Their morphology, formation, and function. *Earth-Science Reviews*, *150*, 285–304. Elsevier B.V. https://doi.org/10.1016/j.earscirev.2015.08.003

Ullman, S. (1979). *The interpretation of structure from motion*. In *Proceedings of the Royal Society of London. Series B, Containing Papers of a Biological Character* (Vol. 203, pp. 405–426). Royal Society (Great Britain). (1153). https://doi.org/10.1098/rspb.1979.0006

Vacchi, M., Gatti, G., Kulling, B., Morhange, C., & Marriner, N. (2022). Climatic control on the formation of marine-notches in microtidal settings: New data from the northwestern Mediterranean Sea. *Marine Geology*, *453*, 106929. https://doi.org/10.1016/j.margeo.2022.106929

Vacchi, M., Ghilardi, M., Melis, R. T., Spada, G., Giaime, M., Marriner, N., et al. (2018). New relative sea-level insights into the isostatic history of the Western Mediterranean. *Quaternary Science Reviews*, *201*, 396–408. https://doi.org/10.1016/j.quascirev.2018.10.025

Vacchi, M., Joyse, K. M., Kopp, R. E., Marriner, N., Kaniewski, D., & Rovere, A. (2021). Climate pacing of millennial sea-level change variability in the central and western Mediterranean. *Nature Communications*, *12*(1), 4013. https://doi.org/10.1038/s41467-021-24250-1

Wolf, J., Woolf, D., & Bricheno, L. (2020). Impacts of climate change on storms and waves relevant to the coastal and marine environment around the UK. *MCCIP Science Review*, 132–157. https://doi.org/10.14465/2020.arc07.saw

19448007, 2024, 6, Downloaded from https://agupubs.onlinelibrary.wiley.com/doi/10.1029/2023GL106829 by CochraneItalia, Wiley Online Library on [19/03/2024]. See the Terms and Conditions (https://onlinelibrary.wiley.com/terms-and-conditions) on Wiley Online Library for rules of use; OA articles are governed by the applicable Creative Commons License